Effect of Cs+ Promoter in Ru/MgO Catalysts

ARTICLE *in* THE JOURNAL OF PHYSICAL CHEMISTRY C · JANUARY 2011

Impact Factor: 4.77 · DOI: 10.1021/jp109737p

1 AUTHOR:

Yurii V. Larichev
Boreskov Institute of Catalysis
24 PUBLICATIONS **196** CITATIONS

SEE PROFILE

Effect of Cs^+ Promoter in Ru/MgO Catalysts

Yurii V. Larichev†

Boreskov Institute of Catalysis, Siberian Branch of Russian Academy of Sciences, Prospekt Akademika Lavrentieva 5, Novosibirsk, 630090, Russia

Received: October 11, 2010; Revised Manuscript Received: November 18, 2010

Ru/MgO and Ru−Cs^+/MgO catalysts were prepared from $Ru(OH)Cl_3$ and were studied by XPS, TEM, CO chemisorption, and EXAFS. An explanation for the large differences in sizes of Ru particles measured by TEM and XRD compared to those determined by CO chemisorption is proposed. This explanation is based on the XPS data that the initial catalyst Ru/MgO consists of Ru^0 metal particles and RuO_2 clusters. The latter are not measured by CO chemisorption and have high stability due to RuO_2−MgO interaction. A new feature of Cs^+ promoter influence on the Ru/MgO catalyst was found. The addition of Cs^+ to the Ru/MgO catalyst, which contains Ru partly in the oxidized form, does not lead to the formation of any cesium ruthenates. Instead, the cesium promoter reduces the RuO_2 clusters, which are stabilized by epitaxy interaction with the support, to form the Ru^0 particles. This new feature of Cs^+ promoter results in the increase of supported Ru useful ratio and Ru-specific surface area in these catalysts.

1. Introduction

Supported ruthenium particles are highly active catalysts for ammonia synthesis or decomposition processes.[1−8] Ammonia decomposition can be one of the prospective ways for production of pure hydrogen for special fuel cell applications.[6−8] The activity of these systems depends on the nature of the Ru precursor. Actually, a Ru catalyst prepared from the usual and cheap precursor $Ru(OH)Cl_3$ has lower activity in the ammonia synthesis/decomposition reactions compared to the Ru catalysts prepared from more expensive and chlorine-free precursors such as $Ru(acac)_3$ (where acac is acetylacetone ligand) or $Ru_3(CO)_{12}$.[9−12] A typical explanation of this fact is a negative influence of residual chlorine ions in Ru catalyst prepared from $Ru(OH)Cl_3$ on the catalytic activity.[9−12]

The use of promoters such as compounds of alkali (or rare-earth) metals results in the increased catalytic activity of Ru catalysts.[1−3,5,8−11,13−16] Due to these alkali promoters, the work function of electron from the Ru nanoparticle surface decreases. For this reason, the rate of N_2 dissociate adsorption on Ru surface increases.[13] Also, according to refs 15 and 16, alkali promoters can remove residual chlorine ions in Ru catalysts.

Recently, it has been shown[17] that the Ru/MgO catalysts prepared from $Ru(OH)Cl_3$ contain some part of the supported Ru in the form of RuO_2. This RuO_2 exists as small clusters with sizes ∼1 nm stabilized by the epitaxy interaction with the support surface. Such epitaxy stabilization allows these RuO_2 clusters to resist hydrogen treatment up to 723 K without reduction. According to our data[17] supported by other studies,[18] Ru catalysts prepared by $Ru(acac)_3$ and $Ru_3(CO)_{12}$, respectively, have no RuO_2 form of Ru. As we see, the oxidation state of supported Ru depends on the type of Ru precursor. For this reason, it is interesting to study the interaction of stabilized RuO_2 nanoclusters with the Cs^+ promoter. How will RuO_2 clusters interact with the Cs^+ promoter?

For example, it was suggested[19] that Ru oxide can transform to cesium ruthenate during the activation of Ru−Cs^+/C catalyst. It is important to verify this hypothesis and find out how the promoter influences the oxidized ruthenium particles.

2. Experimental Section

2.1. Sample Preparation. The MgO support with 200 m^2/g surface area was prepared by precipitation from aqueous $Mg(NO_3)_2$ solution with KOH, followed by drying in air and calcination in dry air flow at 723 K for 2 h. The active component precursor $Ru(OH)Cl_3$ was supported by incipient wetness impregnation from the acetone solution. The precursor concentration was 25 mg/mL. Immediately after the impregnation solution was added to the support, the solvent was removed by blowing air to obtain the air-dry sample. Subsequently, the sample was evacuated at room temperature for 2 h and then at 50 °C for another 2 h. Due to the low solubility of the precursors in acetone, the impregnation procedure was repeated twice. After that, the sample was heated in flowing hydrogen to 450 °C for 2.5 h, and reduced under these conditions for another 6 h. The promoter precursor (Cs_2CO_3) was deposited onto the Ru/MgO sample by incipient wetness impregnation from the solution in anhydrous ethanol at 70 °C. The solvent was removed by blowing argon through the sample. The air-dry sample was evacuated at room temperature for 2 h and then at 50 °C for another 2 h. Another three impregnation cycles were conducted because of the low Cs_2CO_3 solubility in anhydrous ethanol. As soon as the impregnation was completed, the sample was evacuated at 50 °C for 6 h, heated in flowing hydrogen to 450 °C for 2.5 h, and calcined under these conditions for another 6 h. All the catalysts after H_2 reduction were transferred from the reactor to glass ampules without exposure to the atmosphere, and stored in the ampules filled with argon.

As a reference sample, 3.5 wt % Cs^+/MgO was prepared by impregnation of MgO with Cs_2CO_3 by the above-described procedure.

The ruthenium and cesium concentrations in the samples determined by X-ray fluorescence technique are reported in Table 1. Ru and Cs contents in the samples were determined with an accuracy of 0.1 wt % Ru.

† E-mail: ylarichev@gmail.com.

10.1021/jp109737p
Published on Web 12/13/2010

TABLE 1: Metal Loading and Nomenclature of Using Samples

sample	Ru (wt %t)	Cs (wt %)	precursors
Ru/MgO	5.0	−	$Ru(OH)Cl_3$
Ru−Cs^+/MgO	4.5	4.5	$Ru(OH)Cl_3$; Cs_2CO_3

The activities of these catalysts were studied in ammonia synthesis reaction. The results of these experiments were published in our previous work.[13]

2.2. Sample Characterization. ***2.2.1. Transmission Electron Microscopy (TEM).*** Supported samples were studied by high-resolution electron microscopy (HREM) to obtain information about their particle sizes and morphology. A transmission electron microscope JEM 2010 with 200 kV acceleration voltage and 0.14 nm resolution was used in the studies. Typical images of investigated samples are shown in Figure 1.

2.2.2. X-ray Powder Diffraction (XRD). X-ray diffraction (XRD) was performed using a HZG-4 X-ray diffractometer with Cu Kα radiation and a graphite monochromator. The data were collected for 5 s per step with step size 0.05° within the range $20° \le 2\theta \le 130°$. The XRD patterns are shown in Figure 2.

2.2.3. CO Chemisorption. Ruthenium dispersion was determined by CO pulse chemisorption at 25 °C using a He flow of 25 mL/min and pulses of 0.09 mL (10% CO in He) using a Micromeritics AutoChem II 2920 unit. Prior to the dispersion analysis, the samples were freshly treated with flowing pure H_2 (25 mL/min) at 473K for 15 min and then flushed with He (25 mL/min). The stoichiometry of Ru/CO = 1 was assumed in the calculations of the metal dispersion.[20]

2.2.4. X-ray Photoelectron Spectroscopy (XPS). The electronic properties of the samples were studied by XPS. The spectra were registered using VG ESCALAB HP electron spectrometer with nonmonochromatic Al Kα irradiation ($h\nu$ = 1486.6 eV, 200 W). The bonding energy scale of the spectrometer was calibrated using the positions of the core levels Au $4f_{7/2}$ (84.0 eV) and Cu $2p_{3/2}$ (932.6 eV). The Mg 2s line from the support with the binding energy 88.1 eV was used to calibrate the photoelectron lines. Ruthenium catalysts reduced with hydrogen were pressed into a Ni grid and placed into the spectrometer pretreatment chamber. During this procedure, the samples were exposed to air for no longer than 5 min. In the pretreatment chamber, the samples were additionally treated with hydrogen under static conditions at 623 K and 0.1 MPa pressure for 1 h. Then, the samples were evacuated to 10^{-5} Pa and transferred to the analytical chamber to register the spectra.

2.2.5. EXAFS. The spectra of the Ru−K edges (transmission) were recorded by the standard procedure[21] at SSRC, Novosibirsk. The EXAFS spectra were treated using the standard procedure by "Viper" code.[22,23] The background was removed by extrapolating the pre-edge region onto the EXAFS region by Victoreen's polynomials. Three cubic splines were used to simulate the smooth part of the absorption coefficient. The inflection point of the edge of the X-ray absorption spectrum was used as the initial point ($k = 0$) of the EXAFS spectrum. The radial distribution function (RDF) was calculated from the EXAFS spectra in $k^3\chi(k)$ as a modulus of Fourier transform at wavenumber intervals 3.5−13.5 $Å^{-1}$. Debye−Waller factors were fixed at 0.005 $Å^2$.

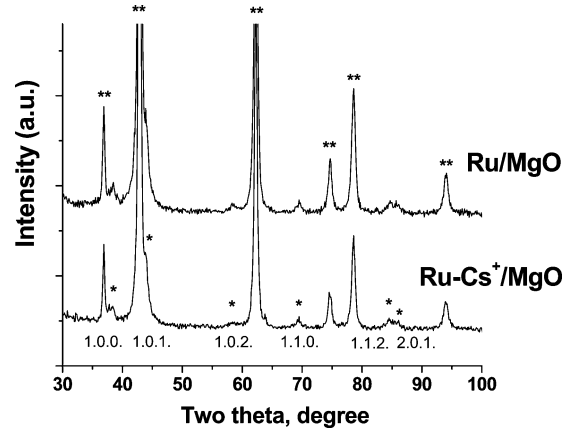

Figure 2. XRD patterns of (top) Ru/MgO and (bottom) Ru−Cs^+/MgO catalysts. The asterisks indicate the Ru reflexes (which have been shown under the bottom curve) and double asterisks indicate MgO reflexes in the XRD patterns.

TABLE 2: Mean Size of Ru Particles Measured by TEM, XRD and CO Chemisorption (nm)

samples	$\langle d_l \rangle$	$\langle d_m \rangle$	$\langle d_{XRD} \rangle$	$\langle d_{CO\ chem.} \rangle$
Ru/MgO	3.5	10.8	10.0	2.9% (34.8 nm)
Ru−Cs^+/MgO	3.2	12.8	9.0	4.9% (20.6 nm)

3. Results

Mean particle diameters[28] (Table 2) were calculated using the TEM images (Figure 1) and the XRD patterns (Figure 2). The TEM data have a good correspondence with the XRD results ($\langle d_m \rangle$ vs $\langle d_{XRD} \rangle$). The obtained data show that the size of Ru particles is almost equal in Ru/MgO and Ru−Cs^+/MgO catalysts (3.2 nm vs 3.5 nm).

However, there is a big difference between the TEM (and XRD) data and the results of the CO chemisorption measurements. According to these results, Ru particles in both catalysts have smaller specific surface areas than can be expected according to the TEM or XRD measurements. Also the CO chemisorption suggests that the specific surface area of Ru particles in the Ru−Cs^+/MgO catalyst is 1.7 times higher than in the Ru/MgO catalyst. This result is very surprising because

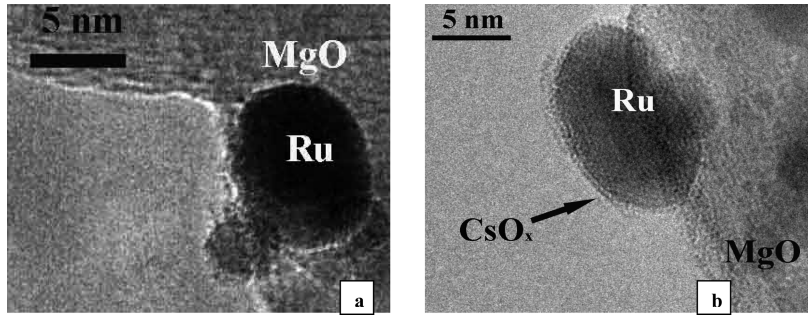

Figure 1. HRTEM micrographs of (a) Ru/MgO and (b) Ru−Cs^+/MgO catalysts. The arrows indicate the cesium-containing layer of disordered structure covering the surface of Ru particles and the areas of the support surface in the closest proximity to the Ru particles.

TABLE 3: Values of Binding Energy Cl $2p_{3/2}$ and Chlorine Content in Samples

sample	E_{bin}(Cl $2p_{3/2}$)	Cl/Mg
Ru/MgO	198.5	0.033
Ru−Cs^+/MgO	198.5	0.037
MgO	198.5	0.003
CsCl	198.0	−
$Ru(OH)Cl_3$	198.2	−

the surface of Ru particles in the Ru−Cs^+/MgO catalyst is covered with a thin layer of the Cs^+ promoter according to TEM data (Figure 1). For this reason, we might expect an opposite effect. Analyzing the XRD data, we could not find any Cs-containing phases in Ru−Cs^+/MgO because the Cs^+ film has very small size for the X-ray diffraction (Figure 2).

The observed Cl 2p signal indicates a small amount of chloride ions present as impurity (Table 3). We observed that after the Ru catalyst preparation the amount of chlorine ions increased. The promotion does not decrease the chlorine amount in the catalyst. The Cl $2p_{3/2}$ binding energies of MgO, Ru/MgO, and Ru−Cs^+/MgO have the value of 198.5 eV. On the other hand, the samples of CsCl and $Ru(OH)Cl_3$ have the values of Cl $2p_{3/2}$ binding energies equal to 198.0 and 198.2 eV, respectively. We can suggest that chlorine ions in Ru catalysts are located on the support and do not react with the Cs^+ promoter or Ru particles.

In our earlier study,[13] it was shown by XPS that Ru−Cs^+/MgO catalysts after reduction by hydrogen contained $Cs_{2+x}O$. After the following exposure to atmospheric oxygen, the cesium suboxide experienced reverse transformation to Cs_2O_2.

For identification of all oxidation states of supported Ru, we used an original technique of difference valence band spectra analysis described elsewhere.[17,24]

Figure 3 shows the difference valence band spectra of Ru catalysts. The left part (Figure 3) presents the difference valence band spectra of Ru/MgO. This spectrum contains the Ru valence band signal and two peaks corresponding to the valence band of RuO_2 clusters.[17] The Ru difference valence band spectra of Ru−Cs^+/MgO is shown in the right part of Figure 3. In this case, we can show that no signal of RuO_2 clusters is present, and this spectrum contains only the Ru valence band signal. That is an interesting effect since it has been shown that ruthenium oxide clusters are very stable and they can resist the hydrogen treatment at 723 K without any decomposition.[17]

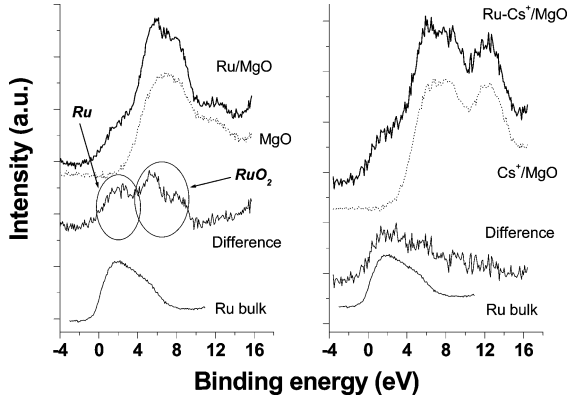

Figure 3. Valence band spectra: (left) Ru/MgO, MgO, difference spectra between Ru/MgO and MgO and Ru bulk; (right) Ru−Cs^+/MgO, Cs^+/MgO, difference spectra between Ru−Cs^+/MgO and Cs^+/MgO and Ru bulk. Ovals show fields corresponding to Ru valence band and RuO_2 valence band.

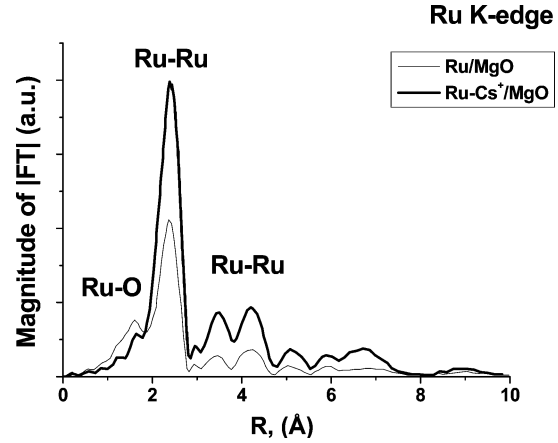

Figure 4. Fourier-transformed radial distribution functions (RDFs) of ruthenium obtained from EXAFS spectra of Ru/MgO (normal curve) and Ru−Cs^+/MgO (bold curve) catalysts.

Apparently this stability can be explained by the epitaxy interaction between {1.1.0.} RuO_2 and {1.0.0.} MgO layers.[25]

So, the Cs^+ promoter has a negative influence on the stability of supported ruthenium oxide clusters. Therefore, instead of possible particles of cesium ruthenates, we found the disappearance of RuO_2 clusters and the presence of Ru metal particles only.

Figure 4 presents the radial distribution functions (RDFs) obtained via Fourier transformation of the EXAFS spectra taken at the Ru K-edge. The RDF for Ru/MgO shows a peak which corresponds to Ru−Ru interactions, a peak due to Ru−O interactions, and a few maxima at longer distances also corresponding to Ru−Ru in the higher shells. The major part of ruthenium is present in the metallic phase. This is proved unambiguously by the comparison of the calculated set of Ru−Ru distances and coordination numbers (Table 4) with those for the metallic Ru reference. Somewhat lower coordination numbers (in comparison to the Ru^0 reference) may be explained by the small particle size (3.5 nm) and the presence of some Ru in the oxidized form. The calculated Ru−O distances are close to those of the bulk ruthenium oxide (RuO_2, Table 4). However, the Ru−Ru distance at ∼3.1 Å characteristic of Ru−O−Ru in bulk RuO_2 is not observed ($N = 0.1$ tabulated in Table 4 is at the detection limit of the method). Hence, bulk ruthenium dioxide is rather unlikely and we infer the formation of small clusters of Ru oxide. This conclusion is in a good agreement with the XPS results.

The Cs^+ promotion of the Ru catalyst results in the decrease of the intensities of the peak corresponding to the Ru−O distances and substantial increase (about 2 times) of the peaks corresponding to the Ru−Ru distance in the all coordination shells compared to the initial Ru/MgO. We do not observe any other peak which can correspond to the Ru oxide cluster interaction with the cesium promoter. Therefore, according to EXAFS data, we also did not find cesium ruthenates in our system.

This fact can be attributed to reduction of Ru oxide clusters to Ru^0 by the promoter influence which is also in a good agreement with the XPS results.

4. Discussion

First of all, we would like to discuss different values of Ru particle sizes in Table 2. Although similar results about big differences (about 3−6 times) between the sizes of Ru particle supported on MgO measured by TEM and H_2 chemisorption

TABLE 4: Distances (*R*) and Coordination Numbers (CN) for Ru Catalyst (As Calculated from Ru K-Edge EXAFS Spectra) and for Ru, RuO_2, and Cs_2RuO_4[a]

	Ru/MgO		$Ru-Cs^+/MgO$		Ru^0		RuO_2		Cs_2RuO_4	
distances	*R* (Å)	CN	*R* (Å)	CN	*R* (Å)	CN	*R* (Å)	CN	*R* (Å)	CN
Ru−O	–	–	–	–	–	–	–	–	1.75	1
Ru−O	1.92	2.2	–	–	–	–	1.92	2	1.76	2
Ru−O	2.03	1.1	–	–	–	–	2.00	4	1.77	1
Ru−Ru	2.61	2.6	2.63	4.8	2.65	6	3.11	2	5.36	2
Ru−Ru	2.72	3.0	2.73	5.0	2.71	6	3.54	8	5.78	2
Ru−Ru	3.76	1.3	3.77	3.2	3.79	6	4.49	4	5.96	2
Ru−Ru	4.26	0.5	4.27	1.0	4.28	2	5.46	8	–	–
Ru−Ru	4.65	3.0	4.65	6.1	4.67	18	5.64	8	–	–
Ru−Cs	–	–	–	–	–	–	–	–	3.75	7
Ru−Cs	–	–	–	–	–	–	–	–	4.74	4

[a] The values of Debye−Waller factors are fixed at 0.005 Å^2. Data for Ru, RuO_2, and Cs_2RuO_4 have been taken from the ICSD Collection database 1997 (Code 23961, Code 43710, and Code 33799, respectively).

were reported earlier,[16] the authors did not give a clear explanation to this fact. They assumed that this effect was related to the presence of residual chlorine ions. According to the XPS data (Table 3), the promotion does not decrease the Cl/Mg ratio but increases the specific surface area of the supported Ru particles (Table 2). Therefore, we assume that this effect is not connected with the residual chlorine ions.

As we mentioned above, the Ru/MgO catalysts prepared from $Ru(OH)Cl_3$ contain some amount of Ru oxide clusters. This fact gave a good explanation for the observed big differences in the Ru particle size measured by TEM and XRD on the one side, and CO chemisorption on the other side. The CO (or H_2) chemisorption technique does not allow determining the specific surface area of Ru oxide nanoparticles.[20,26,27] Therefore, this method shows a lower value of particle sizes compared to TEM and XRD data. The case of $Ru-Cs^+/MgO$ catalyst is more complicated. We know (Figure 1) that the promoter partially covers the surface of the Ru particles. So, we can expect additional decrease of the Ru surface area measured by the CO chemisorption method.[18] However, the experimental data show that the Ru specific surface area in the $Ru-Cs^+/MgO$ sample is higher than the corresponding initial value for Ru/MgO. According to the XPS and EXAFS data, we can conclude that Ru oxide clusters in $Ru-Cs^+/MgO$ are reduced to the Ru particles. The reduction of the Ru oxide clusters to the Ru^0 increases the Ru surface area measured by the CO chemisorption. So, we have two processes, which have an opposite influence on the Ru surface area. The summarized effect of these opposite contributions leads to the increase of the Ru surface area in $Ru-Cs^+/MgO$ compared to Ru/MgO.

So, it is important to pay attention to the possible formation of very small oxide nanoparticles when a big difference between the nanoparticle sizes measured by TEM and chemisorptions technique takes place.

As it was mentioned in refs 17 and 25, Ru oxide cluster is very stable to the H_2 reduction because of the epitaxy interaction between {1.1.0.} RuO_2 and {1.0.0.} MgO layers. Thus, an epitaxy between RuO_2 and MgO can stabilize RuO_2 oxide clusters during hydrogen treatment.

What happens in the case of $Ru-Cs^+/MgO$? How can cesium ions influence this interaction?

We propose the following simple scheme:

$$RuO_2 + Cs_{2+x}O = Ru + Cs_2O$$

$$Cs_2O + H/Ru = Cs_{2+x}O + Ru$$

According to ref 13, cesium in this system is present in suboxide form ($Cs_{2+x}O$, where is $x > 0$). This cesium compound has very big reductive power and can reduce Ru oxide cluster to the Ru^0 despite its epitaxy interaction with the support. During the hydrogen treatment, cesium oxide can transform to cesium suboxide again due to atomic hydrogen adsorbed on the Ru surface. So, we have not found cesium ruthenate formation in $Ru-Cs^+/MgO$. We can conclude that the promotion with Cs^+ contributes to the reduction Ru oxide cluster to Ru^0.

5. Conclusions

The Ru/MgO and $Ru-Cs^+/MgO$ catalysts prepared from $Ru(OH)Cl_3$ have been studied by XPS, TEM, CO adsorption, and EXAFS. A good explanation for the big differences in the sizes of Ru particles measured by TEM and XRD compared to those determined by the CO chemisorption was proposed. This statement based on the XPS data explains that the initial catalyst Ru/MgO consists of Ru^0 metal particles and RuO_2 clusters, which are not measurable by the CO chemisorption and have high stability due to the RuO_2-MgO interaction. The analysis of the XPS spectra of valence zone and EXAFS data shows that the addition the Cs^+ promoter can break the interaction between the support and the RuO_2 clusters. Instead of possible formation of cesium ruthenates, we found that RuO_2 clusters reduced to the Ru particles despite its high stability on MgO support. This new feature of the Cs^+ promoter results in the increase of the useful part of the supported Ru metal and Ru specific surface area in these catalysts. So, the cesium promoter has a multifactor action on supported Ru catalysts.

Acknowledgment. The author is grateful to B. L. Moroz for assistance in the synthesis of the samples, to L. B. Okhlopkova and A.S. Lisitsyn for assistance in the investigation of the samples by CO chemisorption and to V. V. Kriventsov for assistance in the investigation of the samples by EXAFS.

References and Notes

(1) Kowalczyk, Z.; Jodzis, S.; Rarog, W.; Zielinski, J.; Pielaszek, J. *Appl. Catal., A* **1998**, *173*, 153.
(2) Li, Z.; Liang, C.; Feng, Z.; Ying, P.; Wang, D.; Li, C. *J. Mol. Catal. A* **2004**, *211*, 103.
(3) Moggi, P.; Predieri, G.; Maione, A. *Catal. Lett.* **2002**, *79*, 7.
(4) Bielawa, H.; Hinrichsen, O.; Birkner, A.; Muhler, M. *Angew. Chem., Int. Ed.* **2001**, *40*, 1061.

(5) Rarog-Pilecka, W.; Szmigiel, D.; Kowalczyk, Z.; Jodzis, S.; Zielinski, J. *J. Catal.* **2003**, *218*, 465.

(6) Ng, P. F.; Li, L.; Wang, S.; Zhu, Z.; Lu, G.; Yan, Z. *Environ. Sci. Technol.* **2007**, *41*, 3758.

(7) Zheng, W.; Zhang, J.; Zhu, B.; Blume, R.; Zhang, Y.; Schlichte, K.; Schlogl, R.; Schuth, F.; Su, D. S. *ChemSusChem.* **2010**, *3*, 226.

(8) Pyrz, W.; Vijay, R.; Binz, J.; Lauterbach, J.; Buttrey, D. J. *Top. Catal.* **2008**, *50*, 180.

(9) Rosowski, F.; Hornung, A.; Hinrichsen, O.; Herein, D.; Muhler, M.; Ertl, G. *Appl. Catal., A* **1997**, *151*, 443.

(10) Murata, S.; Aika, K. *J. Catal.* **1992**, *136*, 110.

(11) Aika, K.; Takano, T.; Murata, S. *J. Catal.* **1992**, *136*, 126.

(12) Narita, T.; Miura, H.; Ohira, M.; Hondou, H.; Sugiyama, K.; Matsuda, T.; Gonzalez, R. D. *Appl. Catal.* **1987**, *32*, 185.

(13) Larichev, Y. V.; Moroz, B. L.; Moroz, E. M.; Zaykovskii, V. I.; Yunusov, S. M.; Kaluzhnaja, E. S.; Shur, V. B.; Bukhtiyarov, V. I. *Kinet. Catal.* **2005**, *46* (6), 891.

(14) Hansen, T. W.; Hansen, P. L.; Dahl, S.; Jacobsen, C. J. H. *Catal. Lett.* **2002**, *84*, 7.

(15) Aika, K.; Shimazaki, K.; Hattori, Y.; Ohya, A.; Ohshima, S.; Shirota, K.; Ozaki, A. *J. Catal.* **1985**, *92*, 296.

(16) Murata, S.; Aika, K. *Appl. Catal., A* **1992**, *82*, 1.

(17) Larichev, Y. V. *J. Phys. Chem. C* **2008**, *112*, 14776.

(18) Zupanc, C.; Hornung, A.; Hinrichsen, O.; Muhler, M. *J. Catal.* **2002**, *209*, 501.

(19) Shitova, N. B.; Dobrynkin, N. M.; Noskov, A. S.; Prosvirin, I. P.; Bukhtiyarov, V. I.; Kochubei, D. I.; Tsyrul'nikov, P. G.; Shlyapin, D. A. *Kinet. Catal.* **2004**, *45* (3), 414.

(20) Anderson, J. R.; *Structure of Metallic Catalysts*; Academic Press: London, 1975.

(21) Kochubey, D. I.; EXAFS spectroscopy of catalysts, Novosibirsk, Nauka, 1992 (in Russian).

(22) Klementiev, K. V. *J. Phys. D: Appl. Phys.* **2001**, *34*, 209.

(23) Klementiev, K. V. Code VIPER for Windows, freeware: www.desy.de/~klmn/viper.html.

(24) Larichev, Y. V.; Netskina, O. V.; Komova, O. V.; Simagina, V. I. *Int. J. Hydrogen Energy* **2010**, *35*, 6501.

(25) Gao, Y.; Bai, G.; Liang, Y.; Dunham, G. C.; Chambers, S. A. *J. Mater. Res.* **1997**, *12* (7), 1844.

(26) Scheiba, F.; Scholz, M.; Cao, L.; Schafranek, R.; Roth, C.; Cremers, C.; Qiu, X.; Stimming, U.; Fuess, H. *Fuel Cells* **2006**, *6*, 439.

(27) Peng, F.; Zhou, C.; Wang, H.; Yu, H.; Liang, J.; Yang, J. *Catal. Commun.* **2009**, *10*, 533.

(28) $\langle d_i \rangle = \sum N_i d_i / \sum N_i$, $\langle d_m \rangle = \sum N_i d_i^4 / \sum N_i d_i^3$, where $\sum N_i$ is the total number of particles measured in the TEM images, i is the summation index. $\langle d_{XRD} \rangle$ is the Ru crystallite size corresponding to the X-ray Ru (001) reflection calculated by the Scherrer equation: $\langle d_{XRD} \rangle) = K\lambda/(b - b_0)\cos\theta$ where λ is the wavelength of the X-rays and θ is one-half of the scattering angle; b and b_0 are the observed and the instrumental half-widths of the peak in the 2θ scale in radians; $K = 1.0$. $\langle d_{XRDCO\ chem} \rangle$ was calculated from the CO chemisorption values assuming spherical metal particles and the stoichiometry of Ru/CO = 1.0.

JP109737P